APPLIED PHYSICS

Hidden CDW states and insulator-to-metal transition after a pulsed femtosecond laser excitation in layered chalcogenide 1T-TaS$_{2-x}$Se$_X$

Kai Sun[1,2], Shuaishuai Sun[1], Chunhui Zhu[1], Huanfang Tian[1], Huaixin Yang[1,2], Jianqi Li[1,2,3]*

The hidden (H) quantum state in 1T-TaS$_2$ has sparked considerable interest in the field of correlated electron systems. Here, we investigate ultrafast switches to stable H charge density wave (H-CDW) states observed in 1T-TaS$_{2-x}$Se$_x$, with x = 0 and 0.5 crystals, upon excitation with a single femtosecond laser pulse. In situ cooling transmission electron microscopy observations, initiated by a single femtosecond laser pumping with a low fluence, reveal a clear transition from a commensurate CDW phase (q_C) to a new CDW order with q_H = (1 − δ)q_C for the H-CDW state (δ = 1/9) accompanied by an evident phase separation. H-CDW domain relaxation then occurs and yields a stable metallic phase under a high-fluence excitation. Furthermore, electrical resistivity measurements show that the notable drop in x = 0 and 0.5 samples associated with the appearance of H-CDW states depend on laser fluence and temperature. These results potentially provide a new perspective on the photodoping mechanism for the emergence of H-CDW states in the 1T-TaS$_{2-x}$Se$_x$ family.

INTRODUCTION

Layered transition-metal dichalcogenides (TMDs) 1T-TaS$_{2-x}$Se$_x$ and 2H-TaS$_2$ have been extensively studied because they exhibit a number of intriguing electronic phases from various textured charge density waves (CDWs) to the Mott insulating states and the superconducting state (*1–5*). Ultrafast laser excitation can temporarily destroy these thermodynamic ground states and result in quasi-equilibrium states, that is, transient states or metastable phases, which are generally reversible, and revert back to the thermal equilibrium states within 10^{-9} to 10^{-3} s (*6–11*), in contrast to the stable photoinduced states in manganite (*12*, *13*) and chalcogenide glasses (*14*). In recent years, ultrafast transitions and relevant structure dynamics have been extensively investigated in TaS$_2$ family (*15–18*). The kinetic process of CDW orders driven by optical excitation revealed that the photoinduced CDW transition follows a distinctly different mechanism from that of the thermally driven equilibrium phase transition. However, previous investigations focused mainly on the reversible transient processes, and the stable photoinduced quantum state in TMDs is rarely studied. Recently, a stable photoinduced hidden (H) electronic state has been found in the Mott insulator 1T-TaS$_2$ (*19*), which is fundamentally different from any other state in the equilibrium phases and attributed to photodoping effects that result in evident changes in the free energy, and brings nonthermodynamic changes of the energy landscape (*16*). In exhibiting unique physical properties, for example, a large drop in electrical resistance, a notable change in optical reflectivity, thermal erasure, and strain/electromagnetic tunable capability (*20–23*), this H state brings huge application potential for memory and modulator devices. Therefore, researchers are investing significant effort to understand the physical mechanism behind this H state.

Here, we investigate the microstructure of the H state in 1T-TaS$_{2-x}$Se$_x$ (x = 0, 0.5) in in situ low-temperature transmission

electron microscopy (TEM). The formation of H state was found to involve multiple steps and was accompanied by an evident phase separation upon a single femtosecond laser pulse excitation. The H-state transition is demonstrated to be a special CDW transition and is therefore labeled an H-CDW state. An H-CDW order with a modulation structure q_H = (1 − δ)q_C is present at low excitation fluence and further alters its orientation with a rotation of ~2° at high excitation fluence. The switching of resistivity is closely related to the pulse fluence and temperature that coincide with the evolution of the H-CDW order. Therefore, we suggest that they share a common formation mechanism, that is, photodoping effects. Our results help to understand the physical mechanism of the emerging H states.

RESULTS AND DISCUSSION

The thermodynamic phases and relevant CDW transitions for 1T-TaS$_{2-x}$Se$_x$ are strongly dependent on the Se contents and temperature (Fig. 1) (*24*). At low temperature, the nearly commensurate CDW (NCCDW) phase with 0 < x < 0.8 is seen to undergo a transition (T_{CCDW}) to the CCDW phase, that is, a Mott insulator with high resistivity. With increasing Se doping, the insulating Mott state disappears gradually and is replaced by a superconducting state that persists over a wide range of compositions 0.8 < x < 1.6, with a dome-like curve delineating the superconducting transition temperature T_c. The temperature dependence of the resistivity for the three samples we used in this work is shown in fig. S1. Both x = 0 and 0.5 samples exhibit high resistivity as well as a phase transition process at low temperature, whereas sample x = 1 presents a superconducting phase. Recent experiments and theories suggest that the Mott gap formed by the ordered star-shaped polarons (star-of-David) is necessary to form the H state under nonequilibrium conditions (*19*, *22*, *25*). Both the x = 0 and 0.5 samples exhibit ultrafast switching from the CCDW phase (Mott state) to the H-CDW state at low temperature. Hence, our investigations were mainly focused on the structural and physical properties of the H states in the x = 0 and 0.5 samples.

[1]Beijing National Laboratory for Condensed Matter Physics, Institute of Physics, Chinese Academy of Sciences, Beijing 100190, China. [2]School of Physical Sciences, University of Chinese Academy of Sciences, Beijing 100049, China. [3]Collaborative Innovation Center of Quantum Matter, Beijing 100084, China.
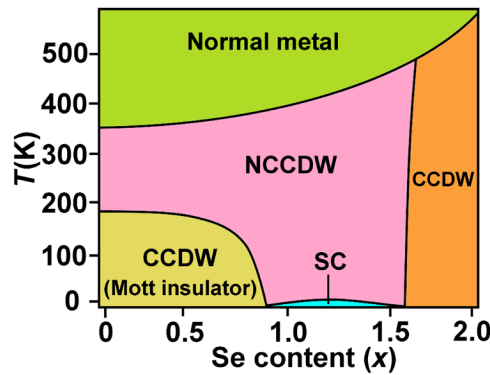*Corresponding author. Email: ljq@aphy.iphy.ac.cn

Fig. 1. Phase diagram of 1T-TaS$_{2-x}$Se$_x$ as a function of temperature and Se content. Three typical samples used in the present study are the Mott insulators with $x = 0$ and 0.5 and the superconductor with $x = 1.0$, as indicated in the diagram.

To reveal directly the microstructure of the H state (H-CDW state), we perform an extensive in situ TEM measurements on 1T-TaS$_{2-x}$Se$_x$ at 10 K, following a single femtosecond laser pulse excitation with various irradiation fluences. Figure 2A shows the original electron diffraction patterns (without laser irradiation) for 1T-TaS$_2$ at 10 K. A series of satellite spots following the main spots arising from CCDW modulations is observed, and further analyses indicate that the atomic configuration in the *a-b* plane for the CCDW phase is well described by a $\sqrt{13}a \times \sqrt{13}a$ supercell that consists of six nearest and six next-nearest Ta neighbors of a central Ta atom, that is, a 13-atom star-of-David cluster of the star-shaped polaron (see the inset of Fig. 2A). All the superstructure spots in this diffraction pattern taken along the [001] zone-axis direction can be indexed by a modulation wave vector $q_C = (3a^* + b^*)/13$ (*15*, *26*).

In Fig. 2 (B and C), the photoinduced alteration of the CDW state is well characterized by evolution of satellite spots around the main reflection. Splitting of the visible spots for the first-order satellites is observed along the modulation direction with a laser fluence of 3 mJ/cm^2. This feature can be defined as a space anomaly for the CDW modulation associated with ultrafast switching to the H-CDW state, which is detailed in the following context. To facilitate comparison, we also analyzed the diffraction patterns by using linear integrals for the first-order satellite spots, yielding a one-dimensional curve in which splitting of the satellite spots can be measured (Fig. 2, E and F), and the coexistence of q_C and q_H suggests a possible phase separation. When we increase the fluence up to 5 mJ/cm^2, the CDW satellite spots are further driven to new positions (Fig. 2C). This CDW modulation shows a clear orientation anomaly with the same modulation period as q_H; therefore, it can be well defined as the second-stage alteration for the H-CDW state contributing to the insulator-to-metal switching produced by the femtosecond laser excitation. Ultimately, the H-CDW order completely reverts to the initial CCDW phase when it is annealed above the Mott insulating transition temperature (Fig. 2D). This behavior of the thermal erasure is discussed systematically below.

The contrast in dark-field imaging from the superstructure satellite spot is quite sensitive to charge-order variations and appears to be the most suitable technique for studying the spatial inhomogeneity of the phase-separated (PS) states (*27*, *28*). Figure 3 presents the dark-field TEM images of the $x = 0$ sample at an identical position under different laser fluences. (The original bright-field image
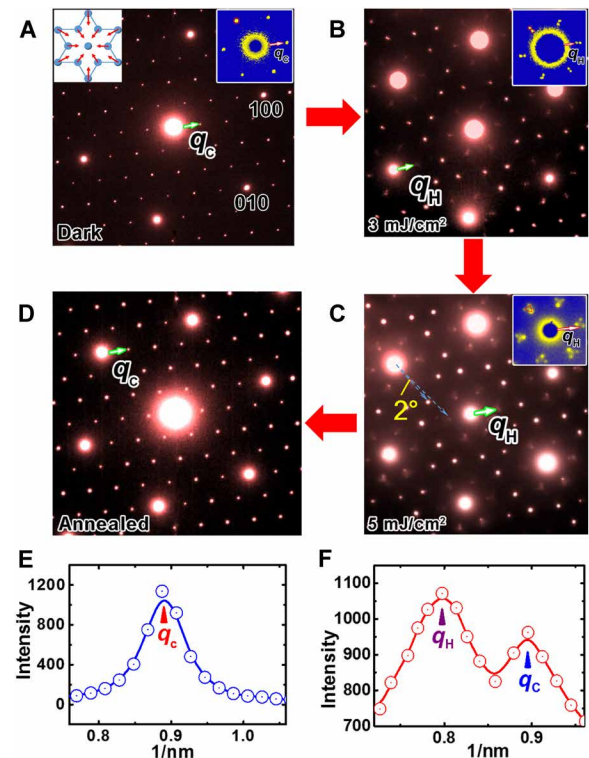

Fig. 2. Alterations of CDW modulation after the pulsed femtosecond-laser excitations. Electron diffraction patterns for the $x = 0$ sample at 10 K along the [001] zone-axis direction demonstrate the structural evolution after femtosecond pulse excitation under (**A**) dark (that is, CCDW phase; a schematic of the star-of-David cluster is exhibited to illustrate the CCDW superstructure), (**B**) 3 mJ/cm^2, and (**C**) 5 mJ/cm^2 and (**D**) upon thermal annealing. The space anomaly and orientation anomaly in H-CDW states are evident following laser excitation. The insets show enlarged diffraction spots to illustrate the positional changes of the CDW satellite spots. At relatively high fluence, an additional orientation anomaly appears in the H-CDW state with a rotation (~2°), as indicated in (C). Linear integrated one-dimensional diffraction curves for the first-order satellite spots of (**E**) CCDW and (**F**) space-anomaly H-CDW state, indicating remarkable changes in the modulation wave vectors.

is shown in fig. S2.) These images were obtained using one of the satellite spots of the (010) main diffraction spot, illustrating the CDW domain evolution at 10 K. The complex contrast can be explained directly as the coexistence of CCDW bright speckles and reordered state (H-CDW state) dark speckles. Figure 3 (B and C) exhibits the visible changes of the spatial contrast variations, especially in the central region of the original image. Obviously, a photoexcitation with a fluence of 3 mJ/cm^2 drives the original CCDW state with uniformly dense bright lamella to an apparently sparse CCDW cluster that appears as a distributed feature alternating with brightness and darkness (inset of Fig. 3B). This nonuniform distribution of the charge-ordered state directly indicates the presence of a phase separation, that is, the H-CDW and the CCDW domains coexisting on the nanoscale in the observed area. Then, the bright lamellas almost vanish under a higher laser fluence of 5 mJ/cm^2, during which the dark speckles become dominant and stable. The CCDW lamellas are demonstrated to decrease predominantly as a result of the femtosecond laser excitation and CDW domain reordering, which can be well interpreted as an increase in the H-CDW
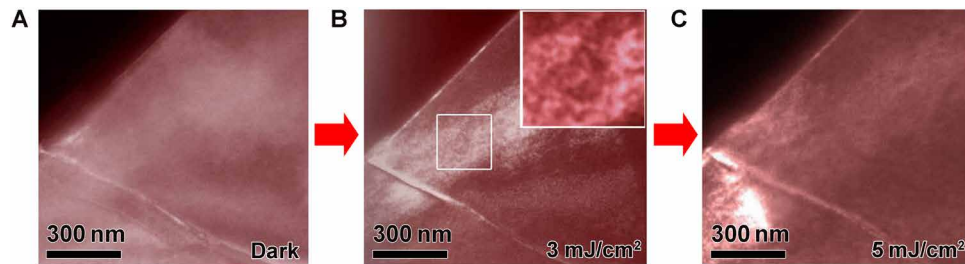
Fig. 3. Microstructural evolutions for CDW domains driven by different laser fluences. Dark-field images for the $x = 0$ sample obtained by the in situ imaging of the CDW satellite spot along [001] zone-axis direction at 10 K under (**A**) dark, showing a homogeneous image contrast, (**B**) 3 mJ/cm², with an inset for an enlarged local area displaying the visible phase separation, and (**C**) 5 mJ/cm², illustrating the variations of PS states and the disappearance of the CCDW domains.

state fraction in the PS state. Generally, upon excitation by an ultrashort laser pulse, electrons and lattice can be driven far from equilibrium, with valence electrons excited to the conduction band. Lattice disordering then appears because of modifications of interatomic forces. In 1T-TaS$_{2-x}$Se$_x$ crystals, photoexcitation initially creates excitation of the charge carriers (that is, electrons and holes), followed by carrier scattering, rapid interband thermalization, and initial CDW melting. The CDW reordering occurs on a time scale of picoseconds (*15*).

To understand the photodoping effect in the emergence of the H-CDW state, Stojchevska *et al.* (*19*) have proposed a structural model arising from the star-shaped polaron cluster reordering (*22*). The stable photoinduced H-CDW state in 1T-TaS$_2$ originates from the presence of the intrinsic band asymmetry and a photodoping effect, which result in the transient imbalance of the photogenerated electron and hole in the Mott ground state. The photodoped hole annihilates localized hexagonal polarons and hence removes the charge at the center of the polaron. Certain voids are expected to aggregate by diffusion into domain walls and then form a new ordered structure of polaron clusters separated by domain walls. Photoexcited electrons could squeeze into the new structure between the polarons, such as interstitials, resulting in an observable metallic state. The fundamental insight of the model is the necessity for a transient electron-hole asymmetry at the Fermi level, which allows a transient photodoping effect to occur just long enough for the H state to form. Once a stable state is established, its collective nature protects it from dissipating.

On the basis of this model, we performed a theoretical analysis to provide a comparison with our experimental results. To perform a qualitative calculation, we used the structural data of the atomic displacements of the CCDW state (*29*). These structural modulations can be expressed as a sinusoidal wave $D(r) = A\sin[2\pi q_C \cdot r + \theta]$, where $D(r)$ is the deviation of the atom from its equilibrium position, A is the amplitude of lattice modulation, r is the atom position vector, and θ is the phase of the modulation. The x-ray diffraction measurements demonstrated that, associated with the CDW wave, the displacements of Ta atoms toward the polaron center are estimated to be about 0.1 Å. We therefore obtained a theoretical diffraction pattern for the CCDW state (Fig. 4A, right). On the basis of the method proposed by McMillan (*30*), the photoinduced space-anomaly H-CDW domain structure can be obtained from our qualitative analysis and calculation (Fig. 4B). In the experimental diffraction pattern (Fig. 2B), we have directly measured the incommensurability (δ) with $\delta = 1/9$, and the modulation wave vector of the H-CDW state can be written as $q_H = (1 - \delta)q_C$. The
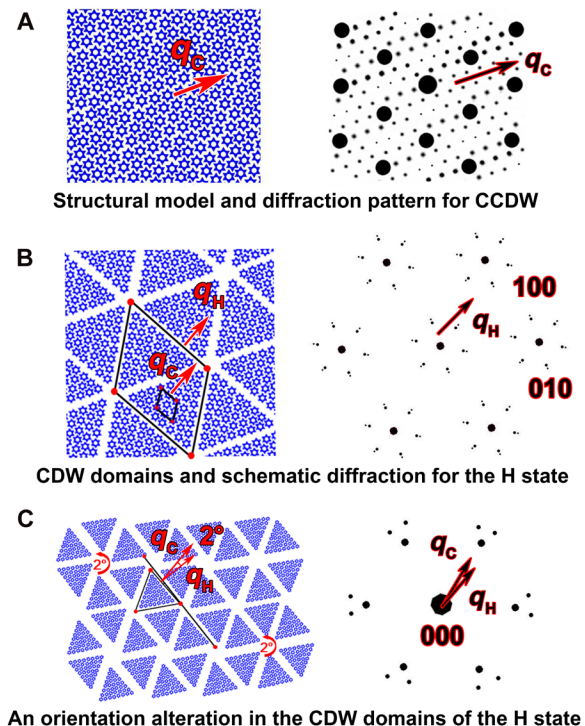

Fig. 4. Structural models and theoretical simulations for typical polaron ordered states. Schematics of the star-shaped polaron order in the *a-b* plane and theoretical (or schematic) diffraction pattern in 1T-TaS$_{2-x}$Se$_x$ for (**A**) the CCDW phase. (**B**) H-CDW domains with $\delta = 1/9$ and schematic diffraction pattern illustrating space anomaly, in agreement with the experimental data of Fig. 2B, in which q_H is parallel to q_C. (**C**) H-CDW domain pattern with structural shearing (~2°) (here, the orientation change is exaggerated for clarity), in which the polaron clusters show a local rotation (~2°) relative to the domain walls, yielding a small direction deviation of q_C and q_H. The diffraction pattern (right column) shows the orientation anomaly for the satellite spots.

modulation vectors of both the CCDW (q_C) and the H-CDW (q_H) states go along the same direction with a slight difference in periodicity (Fig. 4B). The average dimension of the space-anomaly H-CDW domains is about $L = 9\lambda_c \cong 4.8$ nm (λ_c is the period of the CCDW wave in the Mott phase) (*31*). According to the photodoping model (*19*), the total concentration of intrinsic defect (n_d) is estimated to be $n_d \approx \delta = 1/9$, where the intrinsic defects ($n_d = n_v - n_i$) are defined by photoexcited electron interstitials (n_i) and voids (n_v).

Upon increasing the excitation fluence, our in situ structural investigation (Fig. 2C) reveals a more dramatic structure transition with a small CDW domain rotation (~2°) with respect to the CCDW modulation (Fig. 4C). This change in CDW modulation orientation can be interpreted as a relaxation of the H-CDW domains driven by an increase in photoexcited carriers and a higher injection energy, indicating the multistep nature of photoinduced switching. The orientation anomaly in the H-CDW state can be well understood as a small angle (~2°) rotation of the local CDW clusters accompanied by an aggregation of intrinsic defects in the CDW domain walls. The structural distortion of the polaron clusters shows up as a change in their orientation, yielding a small deviation in direction of the modulation vectors of the CCDW (q_C) and H-CDW (q_H) states (Fig. 4C). The schematic of diffraction pattern features this visible orientation anomaly for the satellite spots, in agreement with that obtained from experimental results (Fig. 2C). It is also noted that a metastable NC* state, as revealed in the ultrafast electron diffraction measurements (16), also shows an orientation anomaly. This NC* phase is a transient state correlated with a rotation of the CDW modulation (q_C). In contrast, structural changes in the stable H-CDW state show up in the spot splitting for q_H and a rotation of the local CDW clusters. In addition, our in situ TEM examination of the excited CDW states for the 1T-TaS$_{1.5}$Se$_{0.5}$ ($x = 0.5$) sample indicates a similar structural change in the CDW ordering (fig. S3).

Moreover, a theoretical study of the total free energy on the photoexcited TaS$_2$ system demonstrated that the variation of excited carrier concentration and its dynamical evolution could result in

the stable H-CDW state (19). The H-CDW domain structures were shown to depend markedly on the concentration of intrinsic defects (that is, the photodoped electrons and voids). Our in situ TEM observations revealed that there are actually two distinct ordered states originating from different injected laser fluences related with photodoping mechanism. Figure S4 shows a schematic diagram for the free energy with energy wells at different laser fluences, qualitatively illustrating the emergence of the space-anomaly and orientation-anomaly H-CDW states.

The appearance of the H-CDW state could result in notable changes in physical properties, as demonstrated by measurements of resistivity and reflectivity (6). Figure 5A shows the temperature dependence of resistivity for 1T-TaS$_2$ ($x = 0$). It has been well demonstrated that this sample features a Mott insulator at low temperatures. Upon heating, the transition from the CCDW phase to the NCCDW phase occurs near 210 K with an abrupt drop in resistivity. Upon cooling, a hysteretic loop appears in association with a first-order transition that shows up as a visible discontinuous change in lattice parameters (29, 32, 33). Figure 5B shows the change in resistivity of a 1T-TaS$_2$ ($x = 0$) sample at 4 K with a 300-fs laser pulse excitation at different fluences. The resistivities decrease considerably, and the sample stays in a stable low-resistance state. Note that the drop in resistivity depends strongly on the applied laser fluence, suggesting a partial switching in this system for the transition from the Mott phase to the H-CDW state. Upon heating, the resistivities merge, with the initial curve corresponding to a thermodynamic characteristic of the NCCDW phase. Furthermore,
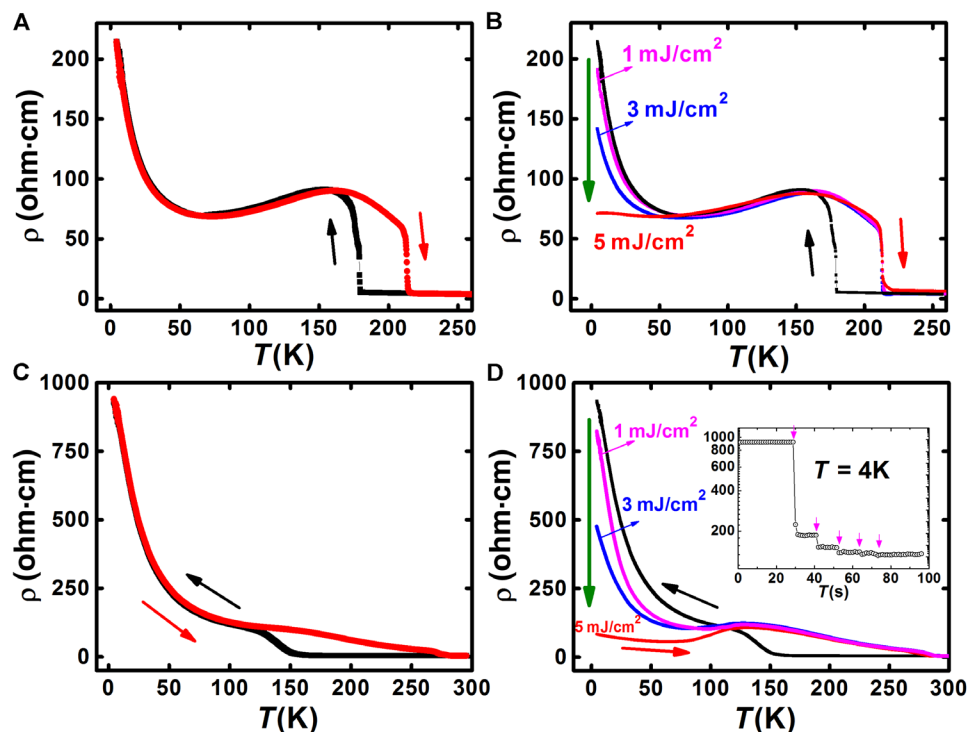
Fig. 5. Temperature dependence of resistivities for various 1T-TaS$_{2-x}$Se$_x$ crystals. (**A**) For the $x = 0$ sample obtained by thermal cycling. (**B**) Resistivity drop (indicated by green arrow) for the $x = 0$ sample at 4 K after a single femtosecond pulse with different fluences. Upon warming, resistivity reverts back at around 100 K. (**C**) Temperature dependence of resistivity for the $x = 0.5$ sample obtained by thermal cycling. (**D**) Photoinduced resistivity drop for the $x = 0.5$ sample at 4 K after a single femtosecond pulse with different fluences. Upon warming, resistivity reverts back near 120 K. The inset shows the time dependence of resistivity at 4 K at a fixed fluence of 5 mJ/cm^2; dynamic saturation is reached for the photoinduced H-CDW state. The arrows indicate a train of femtosecond pulse irradiations.

we performed an experimental measurement of the $x = 0.5$ sample, which also features a Mott insulator at low temperatures. Figure 5C shows the temperature dependence of resistivity over a thermal cycle for the 1T-TaS$_{1.5}$Se$_{0.5}$ crystal. Occurring around 150 K, the transition from the NCCDW to the CCDW phase exhibits a clear hysteresis. Figure 5D shows the resistivity switches in the $x = 0.5$ sample as a result of 300-fs single laser pulse excitation with different fluences. The largest resistivity drop is nearly an order of magnitude down and remains stable in the low-resistance state. Upon heating, they revert to the initial curve for the thermodynamic NCCDW phase around 120 K.

The laser-fluence dependence of resistance switching correlates essentially with the photodoping mechanism. Therefore, we further investigated the photodoping effect and its relevant dynamics upon discrete multipulse photoexcitations. The inset of Fig. 5D shows that a minimum resistivity is reachable following a few separated femtosecond laser pulse excitations in association with a saturation state for the imbalanced electron-hole populations in the H-CDW state. The saturated low-resistance state was achieved after four pulses with a fixed fluence of 5 mJ/cm^2 at 4 K. To eliminate the heat accumulation and achieve full relaxation of each excitation in this measurement, a pulse interval of 10 s was set. This behavior is fundamentally consistent with the photodoping mechanism for the H-CDW state (19, 21). Analyses concerning the structural evolution and resistivity switching suggest that the PS state produced by low-fluence photodoping (Fig. 3B) contributes to a partial switching and lowers electrical resistivity. A full H-CDW state with a minimum resistivity can be reached with high-fluence photodoping and can drive the system into a metallic phase. This suggests that a sufficient population of carrier excitation and H-CDW domain relaxation may have important implications in the ultrafast switching for a stable H-CDW state in the electron crystal.

In the present system, photoinduced switching to the H-CDW state involves two competing mechanisms: photodoping related with light pulses and thermal erasure arising from heat accumulation associated with electron-phonon coupling. A single femtosecond laser pulse can generate nonequilibrium electron-lattice states while barely contributing to any heat accumulation that would drive a thermal relaxation. It was demonstrated experimentally that the H-CDW state could be erased by a train of femtosecond laser pulse radiation, a pulsed electrical current, or a temperature rise (19). These behaviors are considered as the effects of lattice thermalization that directly results in the collapse of the H-CDW state. In our experiments, we performed photoexcitation experiments applying multipulsed laser irradiation of the $x = 0.5$ sample at 4 K (Fig. 6A). Remarkably, different resistivities for the H-CDW states were obtained. This behavior is illustrated by the relative ratio of resistivity changes, $\eta = \Delta R_{4K}/R_{4K}$, where R_{4K} is the resistivity of the sample at 4 K, and ΔR_{4K} is the photoinduced drop of R_{4K} ($R_{Mott} - R_H$) (see inset of Fig. 6A). A maximum η (~95%) is observed under a two-pulse irradiation and then decreases under multiple-pulse irradiation within 0.01 s (shutter time). This result suggests that photoexcitation at relatively higher repetition frequencies would result in a heat accumulation in the crystal, contributing to a partial thermal erasure of the H-CDW state. Figure 6B shows single-pulse ultrafast switching to the H-CDW states for the $x = 0.5$ sample at different experimental temperatures. It is clear that the H-CDW states are induced and remain stable at temperatures from 28 K down to 4 K, and they all revert back upon warming (at ~120 K). In
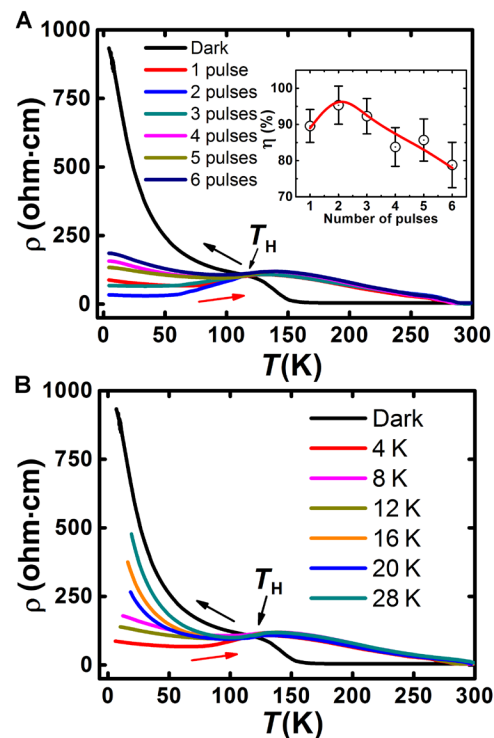

Fig. 6. Resistivity drop under different experiment conditions. (**A**) Drops in resistivity for the $x = 0.5$ sample at 4 K induced by different numbers of laser pulses within 0.01 s (shutter time); upon warming, resistivities revert back to the thermal equilibrium state at approximately 120 K. The inset shows the rate of resistivity change at 4 K ($\eta = \Delta R_{4K}/R_{4K}$), obtained under different numbers of laser pulses within 0.01 s. (**B**) Drops in resistivity induced by a single femtosecond pulse for the $x = 0.5$ sample at different temperatures.

general, it is shown that the photoinduced resistivity drop increases with lowering temperature due to the decrease of thermal erasure effects. It is also noted that the thermal fluctuation at low temperatures could occasionally yield resistivity alterations following the photoexcitation, for example, the resistivity drop at 16 K is slightly smaller than that at 20 K. Note that there is a critical temperature T_H (~120 K) (Fig. 6, A and B) at which all H-CDW resistivity curves revert back to the resistivity of the thermal equilibrium phase. The presence of T_H seems to be essentially associated with the Mott transition (Fig. 1), and the H-CDW state thus exists only below T_H. In contrast, the $x = 1$ sample features a superconducting phase instead of a Mott insulator at low temperatures and does not show any resistivity switching in ultrafast photoexcitation measurements (see fig. S5), indicating that the Mott ground state plays a critical role for the emergence of the H-CDW state.

CONCLUSION

Ultrafast switching from the insulating Mott ground state (CCDW phase) to the stable H-CDW states produced by a single femtosecond laser pulse at low temperatures has been investigated in the layered chalcogenide 1T-TaS$_{2-x}$Se$_x$ samples, with $x = 0$ and 0.5. In situ TEM structural investigations demonstrate that the CCDW state is optically driven into a H-CDW domain structure displaying a space anomaly or an orientation anomaly, accompanied by an observable

evolution of the PS states that depends on the injected laser fluence. The photodoping concentration (n_d) in the H-CDW state is estimated to be about 1/9 associated with structural domains of stacking star-shaped polaron clusters. Our structural analysis of the H-CDW state reveals a multistep nature and H-CDW domain relaxations related with the polaron clusters following changes in laser fluence. Furthermore, for the $x = 0.5$ crystal, the photoinduced appearance of the H-CDW state produces a distinct resistivity drop that exceeds 95% at 4 K. The fluence dependence implies a photodoping mechanism governing the photoinduced transition. The large resistivity switching and stability of the H state in 1T-TaS$_{2-x}$Se$_x$ are expected to have technological applications in high-speed nonvolatile memory devices.

MATERIALS AND METHODS

High-quality single crystals of 1T-TaS$_{2-x}$Se$_x$, with $x = 0$, 0.5, and 1.0, were grown using a standard chemical vapor transport method, and their quality was well characterized as reported in (24). Figure S6 depicts a schematic of our experimental setup for photoexcitation measurements. The resistance measurement devices used in our study are inline with a four-dimensional ultrafast TEM (UTEM). The laser source can concurrently take measurements of physical properties and in situ UTEM microstructure observations. A focused light beam with a spot size of ~80 μm illuminated the sample through a high-transmittance (~95%) optical window and a high-reflectance (~98%) mirror equipped in the TEM; thus, the light fluence on the sample is almost the same as the measured values. The in situ TEM investigations were performed using the UTEM equipped with a liquid helium cooling holder. The single-crystalline samples (about 50 nm thick) were cleaved using adhesive tape and then mounted on the TEM copper grids for observations of the CDW transitions induced by laser pumping. The inset of fig. S6 (top left corner) presents a schematic of the experimental setup depicting the crystal sample and contacts for resistance measurements and photoinduced switching. The exfoliated single-crystalline samples (~100 to 150 nm thick) used in our study were adhered to a sapphire substrate. The resistances were obtained by the standard four-probe method in a vacuum cryostat with a fused silica optical window (transmittance is ~95% for visible light). A 300-fs laser source operating at a wavelength of 520 nm incident from the back side of the sample through the sapphire substrate achieved uniform normal illumination and ensured that there were no unilluminated gaps between the electrodes and the sample.

SUPPLEMENTARY MATERIALS

Supplementary material for this article is available at http://advances.sciencemag.org/cgi/content/full/4/7/eaas9660/DC1

Fig. S1. Resistivity curves for the samples used in this study.
Fig. S2. TEM bright-field image of 1T-TaS$_2$.
Fig. S3. In situ observation for the electron diffraction patterns of 1T-TaS$_{1.5}$Se$_{0.5}$.
Fig. S4. CDW free energy schematic.
Fig. S5. Resistivity curve of 1T-TaSSe with photoexcitation.
Fig. S6. Schematic diagram of the experimental setup.

REFERENCES AND NOTES

1. L. F. Mattheiss, Band structures of transition-metal-dichalcogenide layer compounds. *Phys. Rev. B* **8**, 3719–3740 (1973).
2. Th. Pillo, J. Hayoz, H. Berger, R. Fasel, L. Schlapbach, P. Aebi, Interplay between electron-electron interaction and electron-phonon coupling near the Fermi surface of 1T–TaS$_2$. *Phys. Rev. B* **62**, 4277–4287 (2000).
3. L. Perfetti, P. A. Loukakos, M. Lisowski, U. Bovensiepen, H. Berger, S. Biermann, P. S. Cornaglia, A. Georges, M. Wolf, Time evolution of the electronic structure of 1T-TaS$_2$ through the insulator-metal transition. *Phys. Rev. Lett.* **97**, 067402 (2006).
4. R. E. Thomson, B. Burk, A. Zettl, J. Clarke, Scanning tunneling microscopy of the charge-density-wave structure in 1T-TaS$_2$. *Phys. Rev. B* **49**, 16899–16916 (1994).
5. H. Luo, W. Xie, J. Tao, H. Inoue, A. Gyenis, J. W. Krizan, A. Yazdani, Y. Zhu, R. J. Cava, Polytypism, polymorphism, and superconductivity in TaSe$_{2-x}$Te$_x$. *Proc. Natl. Acad. Sci. U.S.A.* **112**, E1174–E1180 (2015).
6. G. Yu, C. H. Lee, A. J. Heeger, N. Herron, E. M. McCarron, L. Cong, G. C. Spalding, C. A. Nordman, A. M. Goldman, Phase separation of photogenerated carriers and photoinduced superconductivity in high-T_c materials. *Phys. Rev. B* **45**, 4964–4977 (1992).
7. K. Takubo, J.-Y. Son, T. Mizokawa, N. Takubo, K. Miyano, Observation of photoinduced phase transition in phase-separated Pr$_{0.55}$(Ca$_{1-y}$Sr$_y$)$_{0.45}$MnO$_3$ thin films via X-ray photoemission spectroscopy. *Phys. Rev. B* **75**, 052408 (2007).
8. A. Cavalleri, Cs. Toth, C. W. Siders, J. A. Squier, F. Ráksi, P. Forget, J. C. Kieffer, Femtosecond structural dynamics in VO$_2$ during an ultrafast solid-solid phase transition. *Phys. Rev. Lett.* **87**, 237401 (2001).
9. H. Okamoto, Y. Ishige, S. Tanaka, H. Kishida, S. Iwai, Y. Tokura, Photoinduced phase transition in tetrathiafulvalene-*p*-chloranil observed in femtosecond reflection spectroscopy. *Phys. Rev. B* **70**, 165202 (2004).
10. S. Koshihara, Y. Tokura, K. Takeda, T. Koda, Dynamics of a photoinduced phase transition in polydiacetylene crystals. *Phys. Rev. B* **52**, 6265–6272 (1995).
11. L. Piazza, C. Ma, H. X. Yang, A. Mann, Y. Zhu, J. Q. Li, F. Carbone, Ultrafast structural and electronic dynamics of the metallic phase in a layered manganite. *Struct. Dyn.* **1**, 014501 (2014).
12. N. Takubo, I. Onishi, K. Takubo, T. Mizokawa, K. Miyano, Photoinduced metal-to-insulator transition in a manganite thin film. *Phys. Rev. Lett.* **101**, 177403 (2008).
13. N. Takubo, Y. Ogimoto, M. Nakamura, H. Tamaru, M. Izumi, K. Miyano, Persistent and reversible all-optical phase control in a manganite thin film. *Phys. Rev. Lett.* **95**, 017404 (2005).
14. A. Zakery, S. R. Elliott, *Optical Nonlinearities in Chalcogenide Glasses and Their Applications* (Springer, 2007).
15. S. Sun, L. Wei, Z. Li, G. Cao, Y. Liu, W. J. Lu, Y. P. Sun, H. Tian, H. Yang, J. Li, Direct observation of an optically induced charge density wave transition in 1T–TaSe$_2$. *Phys. Rev. B* **92**, 224303 (2015).
16. T.-R. T. Han, F. Zhou, C. D. Malliakas, P. M. Duxbury, S. D. Mahanti, M. G. Kanatzidis, C.-Y. Ruan, Exploration of metastability and hidden phases in correlated electron crystals visualized by femtosecond optical doping and electron crystallography. *Sci. Adv.* **1**, e1400173 (2015).
17. K. Haupt, M. Eichberger, N. Erasmus, A. Rohwer, J. Demsar, K. Rossnagel, H. Schwoerer, Ultrafast metamorphosis of a complex charge-density wave. *Phys. Rev. Lett.* **116**, 016402 (2016).
18. S. Vogelgesang, G. Storeck, J. G. Horstmann, T. Diekmann, M. Sivis, S. Schramm, K. Rossnagel, S. Schäfer, C. Ropers, Phase ordering of charge density waves traced by ultrafast low-energy electron diffraction. *Nat. Phys.* **14**, 184–190 (2018).
19. L. Stojchevska, I. Vaskivskyi, T. Mertelj, P. Kusar, D. Svetin, S. Brazovskii, D. Mihailovic, Ultrafast switching to a stable hidden quantum state in an electronic crystal. *Science* **344**, 177–180 (2014).
20. I. Vaskivskyi, I. A. Mihailovic, S. Brazovskii, J. Gospodaric, T. Mertelj, D. Svetin, P. Sutar, D. Mihailovic, Fast electronic resistance switching involving hidden charge density wave states. *Nat. Commun.* **7**, 11442 (2016).
21. S. Brazovskii, Modeling of evolution of a complex electronic system to an ordered hidden state: Application to optical quench in 1T-TaS$_2$. *J. Superconduct. Novel Magn.* **28**, 1349–1353 (2014).
22. I. Vaskivskyi, J. Gospodaric, S. Brazovskii, D. Svetin, P. Sutar, E. Goreshnik, I. A. Mihailovic, T. Mertelj, D. Mihailovic, Controlling the metal-to-insulator relaxation of the metastable hidden quantum state in 1T-TaS$_2$. *Sci. Adv.* **1**, e1500168 (2015).
23. D. Svetin, I. Vaskivskyi, P. Sutar, E. Goreshnik, J. Gospodaric, T. Mertelj, D. Mihailovic, Transitions between photoinduced macroscopic quantum states in 1T-TaS$_2$ controlled by substrate strain. *Appl. Phys. Exp.* **7**, 103201 (2014).
24. Y. Liu, R. Ang, W. J. Lu, W. H. Song, L. J. Li, Y. P. Sun, Superconductivity induced by Se-doping in layered charge-density-wave system 1T-TaS$_{2-x}$Se$_x$. *Appl. Phys. Lett.* **102**, 192602 (2013).
25. M. Yoshida, R. Suzuki, Y. Zhang, M. Nakano, Y. Iwasa, Memristive phase switching in two-dimensional 1T-TaS$_2$ crystals. *Sci. Adv.* **1**, e1500606 (2015).
26. T. Ritschel, J. Trinckauf, K. Koepernik, B. Büchner, M. V. Zimmermann, H. Berger, Y. I. Joe, P. Abbamonte, J. Geck, Orbital textures and charge density waves in transition metal dichalcogenides. *Nat. Phys.* **11**, 328–331 (2015).
27. J. Q. Li, C. Dong, L. H. Liu, Y. M. Ni, Reentrant charge-ordering transition and phase separation in the layered perovskite La$_{2-2x}$Sr$_{1+2x}$Mn$_2$O$_7$. *Phys. Rev. B* **64**, 174413 (2001).

28. T. Tsurui, J. Kawamura, Nanoscale phase separation of CuI–Cu$_2$MoO$_4$ superionic conducting glass studied by analytical transmission electron microscopy. *J. Non Cryst. Solids* **357**, 132–135 (2011).

29. C. B. Scruby, P. M. Williams, G. S. Parry, The role of charge density waves in structural transformations of 1*T* TaS$_2$. *Philos. Mag.* **31**, 255–274 (1975).

30. W. L. McMillan, Theory of discommensurations and the commensurate-incommensurate charge-density-wave phase transition. *Phys. Rev. B* **14**, 1496–1502 (1976).

31. J. A. Wilson, F. J. Di Salvo, S. Mahajan, Charge-density waves and superlattices in the metallic layered transition metal dichalcogenides. *Adv. Phys.* **24**, 117–201 (1975).

32. J. A. Wilson, F. J. Di Salvo, S. Mahajan, Charge-density waves in metallic, layered, transition-metal dichalcogenides. *Phys. Rev. Lett.* **32**, 882–885 (1974).

33. A. W. Tsen, R. Hovden, D. Wang, Y. D. Kim, J. Okamoto, K. A. Spoth, Y. Liu, W. Lu, Y. Sun, J. C. Hone, L. F. Kourkoutis, P. Kim, A. N. Pasupathy, Structure and control of charge density waves in two-dimensional 1T-TaS$_2$. *Proc. Natl. Acad. Sci. U.S.A.* **112**, 15054–15059 (2015).

Science Advances

Hidden CDW states and insulator-to-metal transition after a pulsed femtosecond laser excitation in layered chalcogenide 1T-TaS$_{2-x}$Se$_x$

Kai Sun, Shuaishuai Sun, Chunhui Zhu, Huanfang Tian, Huaixin Yang and Jianqi Li

ARTICLE TOOLS	http://advances.sciencemag.org/content/4/7/eaas9660
SUPPLEMENTARY MATERIALS	http://advances.sciencemag.org/content/suppl/2018/07/16/4.7.eaas9660.DC1
REFERENCES	This article cites 32 articles, 6 of which you can access for free http://advances.sciencemag.org/content/4/7/eaas9660#BIBL
PERMISSIONS	http://www.sciencemag.org/help/reprints-and-permissions

Use of this article is subject to the Terms of Service